Massive Stars Across Redshifts in the Era of JWST and Large Surveys
Proceedings IAU Symposium No. 402, 2026
A. Wofford, N. St Louis, M. García, S. Simón-Díaz & L. M. Oskinova, eds.
doi:10.1017/S1743921325103931

Investigating chemically homogeneous evolution as a possible source of the 35 $M_\odot$ peak

Lucas M. de Sá[1,2,3], Lieke A. C. van Son[2,4,5] and Matteo Cantiello[2,4]

[1]Instituto de Astronomia, Geofísica e Ciências Atmosféricas, Universidade de São Paulo, Rua do Matão, 1226, São Paulo, SP 05508-090, Brazil
email: lucas.desa@uni-heidelberg.de

[2]Center for Computational Astrophysics, Flatiron Institute, 162 Fifth Avenue, New York, NY 100010, USA

[3]Universität Heidelberg, Zentrum für Astronomie, Institut für Theoretische Astrophysik, Albert Ueberle Str. 2, 69120, Heidelberg, Germany

[4]Department of Astrophysical Sciences, Princeton University, 4 Ivy Lane, Princeton, NJ 08544, USA

[5]Department of Astrophysics/IMAPP, Radboud University, P.O. Box 9010, NL-6500 GL Nijmegen, The Netherlands

Abstract. The $M_1 \sim 35\,M_\odot$ peak has been one of the most consistent features of gravitational-wave data on binary black hole (BBH) mergers, but its astrophysical origins remain among the most elusive. We examine chemically homogeneously evolving (CHE) stars as a plausible origin. CHE stars mix efficiently due to their rapid rotation, and end their Main Sequence evolution as compact helium stars. Efficient mixing occurs only in stars whose zero-age main-sequence masses exceed about $20\,M_\odot$. As a result, CHE stars can form close pairs of massive black holes without undergoing mass transfer, retaining much of their mass and making them natural candidates for BBH mergers near the $35\,M_\odot$ peak. We develop large grids of CHE star simulations using `MESA` to create synthetic populations of BBH mergers. We qualitatively discuss how a combination of the initial mass function and Wolf-Rayet winds can conspire to produce a $\sim 35\,M_\odot$ peak.

Keywords. massive stellar evolution, binary evolution, black hole-black hole mergers

1. Introduction

The recent release of the fourth Gravitational-Wave Transient Catalog (GWTC-4) has brought the number of detected binary black hole (BBH) mergers to over 150 (The LIGO-Virgo-KAGRA Collaboration 2025), affirming the presence of a $M_1 \sim 35\,M_\odot$ peak for BBHs. Although one of the most robustly inferred features of gravitational-wave (GW) data, the $\sim 35\,M_\odot$ peak still lacks a satisfactory explanation (e.g., Roy et al. 2025, and references therein).

We explore one possible formation channel: chemically homogeneously evolving (CHE) stars. Characterized by rapid rotation rates and low metallicities, these stars have been proposed to develop meridional currents that efficiently mix material throughout the envelope (e.g., Yoon and Langer 2005; Yoon et al. 2006). As a result, they become He-enriched on the surface by the end of the Main Sequence (MS), and remain compact throughout their lives. Because the necessary rotation is assumed to develop from tidal locking in tight binaries, these factors make them good potential BBH progenitors

© The Author(s), 2026. Published by Cambridge University Press on behalf of The International Astronomical Union. This is an Open Access article, distributed under the terms of the Creative Commons Attribution licence (https://creativecommons.org/licenses/by/4.0/), which permits unrestricted re-use, distribution and reproduction, provided the original article is properly cited.

https://doi.org/10.1017/S1743921325103931 Published online by Cambridge University Press

(Mandel and de Mink 2016; Marchant et al. 2016). They are furthermore expected to lead to more massive BBHs ($M_1 \gtrsim 20\,M_\odot$) because rotational mixing is only effective in more massive, radiation-dominated stars (Hastings et al. 2020), and because their compactness avoids mass transfer episodes, potentially allowing them to retain a larger fraction of their initial mass. Finally, CHE mostly forms equal-mass binaries (though mass ratios as low as $q \approx 0.7$ might occur in $\sim 20\%$ of systems, see Marchant et al. 2016; Hastings et al. 2020), which is also in line with recent findings on the $M_1 \sim 35\,M_\odot$ peak (Roy et al. 2025; Banagiri et al. 2025).

2. MESA setup

We run grids of CHE star models with version 23.04.1 of the 1D stellar structure code Modules for Experiments in Stellar Astrophysics (`MESA`, Paxton et al. 2011, 2013, 2015, 2018, 2019; Jermyn et al. 2023). We build our models based on the inlists and extra routines from Gottlieb et al. (2024), with the $\sigma = 0$ $^{12}C(\alpha,\gamma)^{16}O$ reaction rate from deBoer et al. (2017) as our fiducial assumption. Besides varying mass, initial spin periods and metallicities, we build an updated wind scheme, with the minimum between Björklund et al. (2023) and Krtička et al. (2024) for thin (OB) winds; Vink et al. (2011) for thick (very massive star, VMS) He-poor winds; and the minimum between Sander and Vink (2020) (with the Sander et al. 2023, temperature correction) and Vink (2017) for thick (Wolf-Rayet, WR) He-rich winds. We transition to thick He-poor winds following the framework by Sabhahit et al. (2023), and to He-rich winds by interpolating between He-poor (either thin OB or thick VMS) and He-rich WR winds within the $Y_{\rm surf} = 0.4 - 0.7$ range. Finally, we adopt rotation-enhanced mass-loss following Heger et al. (2000).

For simplicity, we run only single stellar evolution models, which we find to allow for CHE for a wide range of zero-age MS (ZAMS) masses and spins. We emulate binary evolution by assuming $q = 1$, tidal synchronization at ZAMS (de Mink et al. 2009) and Jeans mode mass loss. Models are run up to core carbon depletion, after which point the star is not expected to lose any significant amount of mass or angular momentum (AM). We define CHE as maintaining $Y_{\rm surf}/Y_{\rm center} \geq 0.7$ throughout the MS, and stop any runs that violate this condition or lead into a stellar merger at ZAMS by overflow through the second Lagrangian point (following Marchant et al. 2016).

Our model grid consists of 20 values of $M_{\rm ZAMS}$, uniformly sampled with step $10\,M_\odot$ between $20 - 120\,M_\odot$, and with step $20\,M_\odot$ between $120 - 300\,M_\odot$; and 36 values of $P_{\rm ZAMS}$, with step 0.05 d between $0.35 - 0.90$ d, step 0.1 d between $0.90 - 2.60$ d, and step 0.2 d between $2.60 - 4.00$ d. Each of the 720 models is evolved for 9 metallicities, $Z/Z_\odot = 1/100, 1/50, 1/20, 1/10, 1/5, 0.4, 0.6, 0.8, 1.0$, bringing the total to 6480 models.

Next, we use these MESA models to estimate a population of merging binary black holes. To this end, we fit three-dimensional linear interpolators on $M_{\rm ZAMS}$, $P_{\rm ZAMS}$ and Z over our `MESA` grids, and re-draw $M_{\rm ZAMS}$ from a Kroupa (2001) IMF, and $P_{\rm ZAMS}$ from a log-uniform distribution. Unless stated otherwise, metallicities are re-drawn from the redshift-dependent skewed-Gaussian distribution from van Son et al. (2023). We compute merger rates from large interpolated populations with a `MESA`-adapted version of `CosmicIntegrator`, part of the post-processing suite of the `COMPAS` binary population synthesis code (Neijssel et al. 2019; Riley et al. 2021).

3. The BBH yield from CHE at fixed metallicity

From our Fiducial model grid, we find that the minimum mass at ZAMS for which CHE occurs is $\sim 30\,M_\odot$ for metallicities below $0.2\,Z_\odot$, and $\sim 50\,M_\odot$ for $Z \geq 0.2$. Fig. 1 shows the resulting final primary mass distribution for six different metallicity ranges,

https://doi.org/10.1017/S1743921325103931 Published online by Cambridge University Press

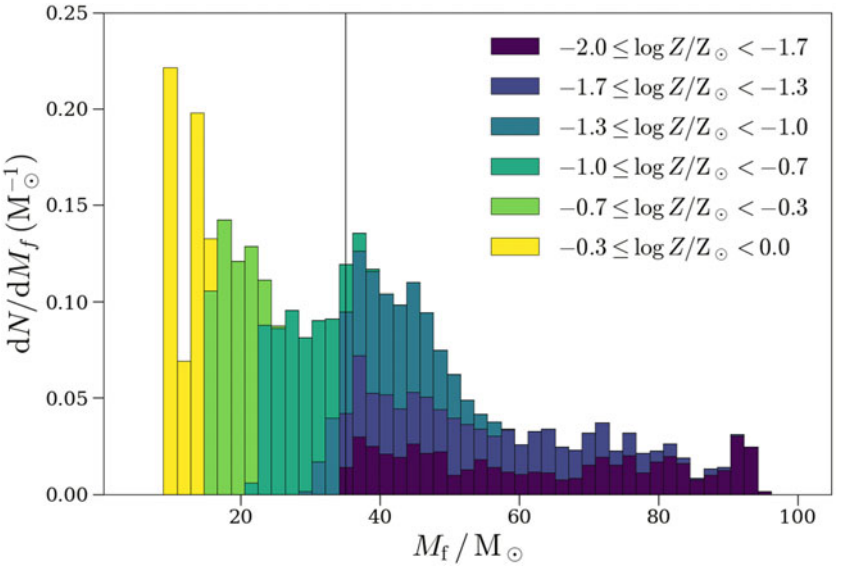


Figure 1. Final mass distribution from an interpolated population of 10^8 binaries over different metallicity intervals, for a population generated following the Kroupa (2001) IMF, a log-uniform orbital period distribution and a log-uniform metallicity distribution. The solid vertical line indicates $M_f = 35\,M_\odot$.

without filtering for delay time, from an interpolated $\sim 10^8$ binary population following a log-uniform metallicity distribution. The effect of increasing wind mass-loss with metallicity is immediately evident, with the high metallicity ($-0.3 \leq \log Z/Z_\odot < 0$) range producing a sharp peak at $\sim 10\,M_\odot$, while the low metallicity ($-2 \leq \log Z/Z_\odot < -1.7$) range produces masses between $\sim 35\,M_\odot$ and $\sim 95\,M_\odot$, with a modest pile-up at the upper end. Conspicuously, all $\log Z/Z_\odot > -0.7$ metallicities produce either a peak or a sharp cut-off around $\sim 35\,M_\odot$ (black vertical line in Fig. 1).

Two main effects shape the distribution in Fig. 1. First is the interplay between the minimal ZAMS mass required for CHE, $m_{\rm CHE}^{\rm min} \approx 30\,M_\odot$, at low metallicities, and the Kroupa (2001) IMF, which favors lower masses. In other words, the initial mass function of CHE stars is itself peaked slightly above the lower edge of the window, i.e., $\sim 35\,M_\odot$. In the absence of mass loss, this means most stars will have a final mass of $\sim 35\,M_\odot$, which leads to the lowest metallicities in Fig. 1 seeing their final masses cut off around that value.

The second effect is the strong wind mass-loss from WR and VMS winds. VMS winds dominate mass-loss at the lowest metallicities, setting the maximum final mass of $\sim 90\,M_\odot$ visible in Fig. 1. At intermediate metallicities, WR (He-rich) winds lead to significant mass-loss even at $< 100\,M_\odot$, narrowing the distribution towards the minimum progenitor mass of $\sim 35\,M_\odot$, where mass-loss becomes weak enough to create a pile-up. At the highest metallicities, the CHE window closes at $M_{\rm ZAMS} \sim 50\,M_\odot$, but mass-loss is so intense that the distribution shifts to create a narrow peak at final masses as low as $\sim 10\,M_\odot$.

4. Merger rates

We draw a new $\sim 10^8$ binary interpolated population, this time sampling from the van Son et al. (2023) metallicity distribution. Fig. 2 shows the resulting BBH merger rates. This demonstrates that our fiducial model peaks at $\sim 35\,M_\odot$ for low redshifts ($0 < z < 1$).

https://doi.org/10.1017/S1743921325103931 Published online by Cambridge University Press

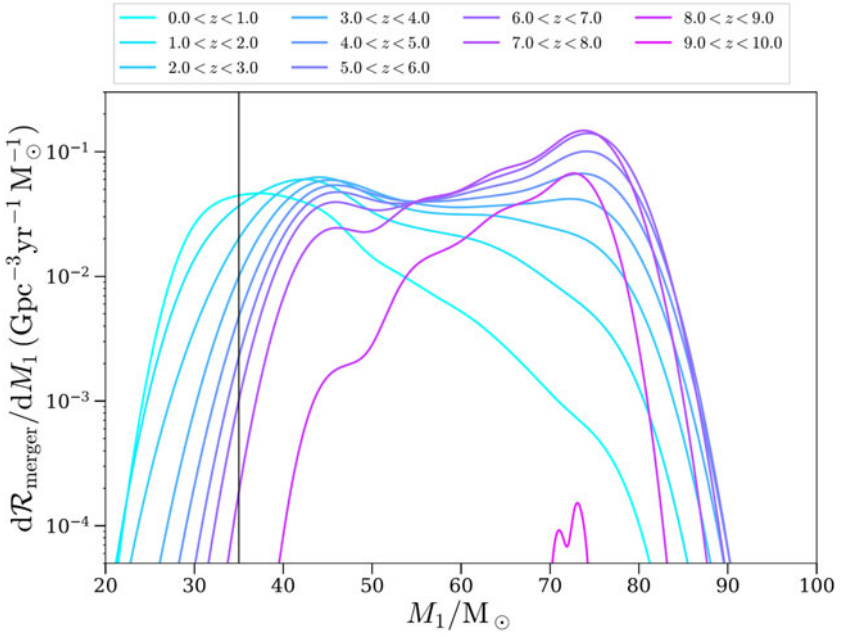


Figure 2. Merger rates over mass, for different redshift bins, for an interpolated 10^8 binary population, drawn from the Kroupa (2001) IMF, a log-uniform orbital period distribution and the metallicity distribution by van Son et al. (2023). The solid vertical line indicates $M_1 = 35\,M_\odot$.

This peak shifts to higher masses with redshift. This is the result of a mass-metallicity-delay time relation: lower metallicities, with weaker winds, favor greater masses and shorter delay times. Thus, the most massive mergers form early (higher redshift) and merge quickly, while the least massive mergers form later (lower redshift) and merge later.

In summary, we find that the CHE channel creates a low-redshift $\sim 35\,M_\odot$ peak hailing from the interplay between the IMF and WR winds; and a high-redshift $\sim 90\,M_\odot$ peak hailing from VMS winds. The distribution shifts smoothly from one to the other with increasing redshift. We note, however, that while our current simulations produce a reasonable match for the peak location, our merger rates are much broader in M_1 than what is supported (see Roy et al. 2025). We conclude that our results suggest *how* CHE might explain a feature at $35M_\odot$, but that our particular assumptions are not fully compatible with observations.

Spins

Another important constraint is that the $\sim 35\,M_\odot$ mergers are consistent with slowly-spinning, $\chi < 0.1$ BHs (Roy et al. 2025). We find our Fiducial grid, which assumes the traditional Tayler-Spruit (TS) dynamo (Spruit 2002), to exclusively result in $\chi > 1$ cores. These are likely to lead to a collapsar and GRB launch, which have been found to be efficient at halting BH spins, but also at unbinding up to $\sim 90\%$ of a WR progenitor's mass (e.g. Gottlieb et al. 2022), which would rule out CHE as the peak progenitor. We re-run a small subset of models with the Fuller and Lu (2022) AM transport prescription, which we find to exclusively produce $\chi < 0.01$ cores. Such a situation allows for the production of the $\sim 35\,M_\odot$ peak. However, we stress that this would eliminate CHE stars as GRB progenitors. Whether AM transport in CHE stars corresponds to either model or has a more moderate efficiency remains unclear, and the problem of spins is left to future work.

https://doi.org/10.1017/S1743921325103931 Published online by Cambridge University Press

5. Conclusions

We have mapped out the conditions under which CHE could be responsible for the $\sim 35\,M_\odot$ peak. In the absence of mass transfer, CHE results in a *(thick) wind-dominated* BBH merger formation channel. Crucially, CHE allows thick WR winds to affect lower progenitor masses, for which VMS winds are not activated, without mass transfer. The bump in merger rates is a reflection of the minimum mass for CHE, at which winds become negligible. We assume the BH mass directly tracks the final progenitor mass. The efficiency of rotational mixing and the nature of CHE star mass-loss are thus the most critical assumptions for CHE. Determining whether CHE stars can simultaneously satisfy the mass and spin constraints required to match the $M_1 \sim 35\,M_\odot$ peak observed in BBH mergers, while also accounting for GRBs, will require further study, leaving CHE as an exciting topic at the intersection between GWs, GRBs and WRs.

References

Banagiri, S., Thrane, E., & Lasky, P. D. 2025, *arXiv e-prints*, arXiv:2509.15646.

Björklund, R., Sundqvist, J. O., Singh, S. M., Puls, J., & Najarro, F. 2023, *A&A*, 676, A109.

de Mink, S. E., Cantiello, M., Langer, N., Pols, O. R., Brott, I., & Yoon, S.-C. 2009, *A&A*, 497(1), 243–253.

deBoer, R. J., Görres, J., Wiescher, M., Azuma, R. E., Best, A., Brune, C. R., Fields, C. E., Jones, S., Pignatari, M., Sayre, D., Smith, K., Timmes, F. X., & Uberseder, E. 2017, *Rev. Mod. Phys.*, 89(3), 035007.

Fuller, J. & Lu, W. 2022, *Monthly Notices of the Royal Astronomical Society*, 511(3), 3951–3964.

Gottlieb, O., Liska, M., Tchekhovskoy, A., Bromberg, O., Lalakos, A., Giannios, D., & Mösta, P. 2022, *ApJL*, 933(1), L9.

Gottlieb, O., Renzo, M., Metzger, B. D., Goldberg, J. A., & Cantiello, M. 2024, *ApJL*, 976(1), L13.

Hastings, B., Langer, N., & Koenigsberger, G. 2020, *Astronomy and Astrophysics*, 641, A86.

Heger, A., Langer, N., & Woosley, S. E. 2000, *ApJ*, 528(1), 368.

Jermyn, A. S., Bauer, E. B., Schwab, J., Farmer, R., Ball, W. H., Bellinger, E. P., Dotter, A., Joyce, M., Marchant, P., Mombarg, J. S. G., Wolf, W. M., Sunny Wong, T. L., Cinquegrana, G. C., Farrell, E., Smolec, R., Thoul, A., Cantiello, M., Herwig, F., Toloza, O., Bildsten, L., Townsend, R. H. D., & Timmes, F. X. 2023, *APJS*, 265(1), 15.

Kroupa, P. 2001, *Monthly Notices of the Royal Astronomical Society*, 322(2), 231–246.

Krtička, J., Kubát, J., & Krtičková, I. 2024, *A&A*, 681, A29.

Mandel, I. & de Mink, S. E. 2016, *Monthly Notices of the Royal Astronomical Society*, 458(3), 2634–2647.

Marchant, P., Langer, N., Podsiadlowski, P., Tauris, T. M., & Moriya, T. J. 2016, *A&A*, 588, A50.

Neijssel, C. J., Vigna-Gómez, A., Stevenson, S., Barrett, J. W., Gaebel, S. M., Broekgaarden, F. S., de Mink, S. E., Szécsi, D., Vinciguerra, S., & Mandel, I. 2019, *MNRAS*, 490(3), 3740–3759.

Paxton, B., Bildsten, L., Dotter, A., Herwig, F., Lesaffre, P., & Timmes, F. 2011, *The Astrophysical Journal Supplement Series*, 192, 3.

Paxton, B., Cantiello, M., Arras, P., Bildsten, L., Brown, E. F., Dotter, A., Mankovich, C., Montgomery, M. H., Stello, D., Timmes, F. X., & Townsend, R. 2013, *The Astrophysical Journal Supplement Series*, 208, 4.

Paxton, B., Marchant, P., Schwab, J., Bauer, E. B., Bildsten, L., Cantiello, M., Dessart, L., Farmer, R., Hu, H., Langer, N., Townsend, R. H. D., Townsley, D. M., & Timmes, F. X. 2015, *The Astrophysical Journal Supplement Series*, 220, 15.

Paxton, B., Schwab, J., Bauer, E. B., Bildsten, L., Blinnikov, S., Duffell, P., Farmer, R., Goldberg, J. A., Marchant, P., Sorokina, E., Thoul, A., Townsend, R. H. D., & Timmes, F. X. 2018, *The Astrophysical Journal Supplement Series*, 234, 34.

https://doi.org/10.1017/S1743921325103931 Published online by Cambridge University Press

Paxton, B., Smolec, R., Schwab, J., Gautschy, A., Bildsten, L., Cantiello, M., Dotter, A., Farmer, R., Goldberg, J. A., Jermyn, A. S., Kanbur, S. M., Marchant, P., Thoul, A., Townsend, R. H. D., Wolf, W. M., Zhang, M., & Timmes, F. X. 2019, *The Astrophysical Journal Supplement Series*, 243, 10.

Riley, J., Mandel, I., Marchant, P., Butler, E., Nathaniel, K., Neijssel, C., Shortt, S., & Vigna-Gómez, A. 2021, *Monthly Notices of the Royal Astronomical Society*, 505(1), 663–676.

Roy, S. K., van Son, L. A. C., & Farr, W. M. 2025, A Mid-Thirties Crisis: Dissecting the Properties of Gravitational Wave Sources Near the 35 Solar Mass Peak.

Sabhahit, G. N., Vink, J. S., Sander, A. A. C., & Higgins, E. R. 2023, *Monthly Notices of the Royal Astronomical Society*, 524(1), 1529–1546.

Sander, A. a. C., Lefever, R. R., Poniatowski, L. G., Ramachandran, V., Sabhahit, G. N., & Vink, J. S. 2023, *A&A*, 670, A83.

Sander, A. A. C. & Vink, J. S. 2020, *Monthly Notices of the Royal Astronomical Society*, 499(1), 873–892.

Spruit, H. C. 2002, *Astronomy and Astrophysics*, 381, 923–932.

The LIGO-Virgo-KAGRA Collaboration 2025, *arXiv e-prints*, arXiv:2508.18082.

van Son, L. A. C., de Mink, S. E., Chruślińska, M., Conroy, C., Pakmor, R., & Hernquist, L. 2023, *ApJ*, 948(2), 105.

Vink, J. S. 2017, *A&A*, 607, L8.

Vink, J. S., Muijres, L. E., Anthonisse, B., de Koter, A., Gräfener, G., & Langer, N. 2011, *A&A*, 531, A132.

Yoon, S.-C. & Langer, N. 2005, *A&A*, 443(2), 643–648.

Yoon, S.-C., Langer, N., & Norman, C. 2006, *A&A*, 460(1), 199–208.

https://doi.org/10.1017/S1743921325103931 Published online by Cambridge University Press